Food and Chemical Toxicology 149 (2021) 112032

Contents lists available at ScienceDirect

Food and Chemical Toxicology

journal homepage: www.elsevier.com/locate/foodchemtox

Structural elucidation of three novel oligosaccharides from Kunlun Chrysanthemum flower tea and their bioactivities

Qian Yu [a,b,1], Wei Chen [a,1], Jing Zhong [a], Degang Qing [c], Chunyan Yan [a,b,*]

[a] Clinical Pharmacy of the First Affiliated Hospital of Guangdong Pharmaceutical University, Guangzhou, 510060, China
[b] School of Clinical Pharmacy, Guangdong Pharmaceutical University, Guangzhou, 510006, China
[c] Xinjiang Institute of Traditional Chinese Medicine and Ethnodrug, Urumqi, 830002, China

ARTICLE INFO

Handling editor. Dr. Jose Luis Domingo

Keywords:
Coreopsis tinctoria
Kunlun chrysanthemum
Oligosaccharides
α-Glucosidase inhibitory activity
α-Amylase inhibitory activity
Anti-neuroinflammation activity

ABSTRACT

Coreopsis tinctoria is commonly called Kunlun Chrysanthemum and a plateau plant with tremendous commercial value in functional tea and medicinal applications. In folk medicine, Kunlun Chrysanthemum flower is often used as an adjunctive therapy for diabetes and Alzheimer's disease. To further explore the chemicals responsible for the health benefits of Kunlun Chrysanthemum flowers, three homogeneous oligosaccharides, CT70-1A, CT70-1B and CT70-2 were isolated, and their detailed structures were determined from chemical and spectral analyses. The three oligosaccharides were composed of glucose, mannose, galactose, and arabinose in different ratios. They showed dose-dependent α-amylase and α-glucosidase inhibitory effects. In addition, they showed NO production inhibitory activities in BV2 cells, with IC_{50} values of 0.23, 0.24 and 0.27 mM, respectively. Taken together, these results suggested that Kunlun Chrysanthemum oligosaccharides might ameliorate hyperglycemia and neuroinflammation, which could prevent the development of diseases such as type 2 diabetes and Alzheimer's disease. This study provides chemical and bioactive perspectives that support the consumption of Kunlun Chrysanthemum flower tea for health benefits.

1. Introduction

Numerous reports indicate that neuroinflammation, characterized by the hyperactivity of microglia, is involved in the pathogenesis of some neurodegenerative diseases, such as Alzheimer's disease (AD), Parkinson's disease, and Huntington's disease (Joakim et al., 2013; Zhang and Jiang, 2015). Excessive microglia activation leads to increased proinflammatory cytokines, including nitric oxide (NO), tumor necrosis factor α (TNF-α), interleukin 1β (IL-1β), and reactive oxygen species (ROS) (Hensley, 2010). These factors may aggravate the progressive damage of neurodegenerative diseases. Therefore, the inhibition of the hyperactivity of microglia, which could suppress the production and secretion of proinflammatory cytokines, may be a potential strategy for the treatment of AD mediated by neuroinflammation (Fang et al., 2018; Zhang et al., 2016). It has been reported that compounds extracted from *Cannabis sativa* Linn. significantly inhibited the TNF-α released from BV2 microglia, suggesting its ability to treat neurodegenerative diseases (Zhou et al., 2018). Moreover, *Ganoderma lucidum* (Leyss. exFr.) Karst polysaccharides were reported to promote neural progenitor cell proliferation, thus enhancing neurogenesis and mitigating the cognitive deficits in mice with AD (Huang et al., 2017).

Diabetes mellitus (DM) is a chronic metabolic disease and a major disorder of insulin regulation. DM, especially type 2 diabetes (T2D), has become a major public health concern. T2D causes serious complications, such as diabetic ketoacidosis, nonketotic hyperosmolar coma, cardiovascular diseases, and chronic kidney failure (Campbell, 2011). Researchers have reported that diabetes increases the risk of AD (Sridhar et al., 2015). The underlying mechanisms are complicated and varied, including inflammation, cerebrovascular changes, the deregulation of brain insulin uptake, and Aβ accumulation (Weinstein et al., 2015; Pasquier et al., 2006). Takeda et al. (2010) used an animal model to investigate the relationship between AD and DM. APP^{+}-*ob/ob* (express amyloid precursor protein with hyperglycemia) mice showed severe cerebrovascular changes and amyloid deposition, while the insulin level in the APP^{+}-*ob/ob* mice brains was significantly lower than that in the control. It could be concluded that cerebrovascular inflammation and alteration in brain insulin signaling may be pivotal factors for AD and DM. Velazquez et al. (2017) also drew the same conclusion. These

* Corresponding author. School of Clinical Pharmacy, Guangdong Pharmaceutical University, Guangzhou, 510006, China.
E-mail address: ycybridge@gdpu.edu.cn (C. Yan).
[1] These authors contributed equally to this work.

https://doi.org/10.1016/j.fct.2021.112032
Received 3 November 2020; Received in revised form 22 December 2020; Accepted 26 January 2021
Available online 30 January 2021

studies suggested that anti-diabetic drugs may have direct implications on the treatment of AD and dementia prevention (Barnes and Yaffe, 2011). Thus, control of hyperglycemia may be an effective way to prevent neurodegeneration (Heneka et al., 2015). As key enzymes, α-amylase and α-glucosidase play important roles in controlling postprandial hyperglycemia and maintaining glucose levels in the normal range. The inhibition of these enzymes will slow down the hydrolysis of carbohydrates, as well as prolong the speed of blood glucose absorption from the small intestine (Joshi et al., 2015). Therefore, the inhibitors of α-amylase and α-glucosidase function as effective drugs to control the blood glucose level and treat T2D. However, these commercial drugs come with some side effects; hence, the search for natural products with enzyme inhibitory effects and minimal side effects are needed (Kwon et al., 2006).

Coreopsis tinctoria Nutt. originates in North America and was introduced into Xinjiang, China. It is now widely distributed in the Kunlun Mountains and is called "Kunlun Chrysanthemum" by the local people. As an industrial crop, Kunlun Chrysanthemum has been cultured on a large scale, with a yield of almost 5000 kg per year. Moreover, it is used as an ingredient in a well-known Compositae functional tea (Wang et al., 2014), and also used to treat cold and fever, apart from removing toxins (Wang et al., 2015). Therefore, it has become a popular herbal product in the health tea/beverage industry in China. Recent pharmacological studies have shown that it has various activities, such as hypoglycemic, hypotensive, and anticancer (Dias et al., 2010; Wang et al., 2014). A previous study reported that ethyl acetate extracts of Kunlun Chrysanthemum flowers significantly controlled the blood glucose levels of the STZ-induced diabetic rats (Yao et al., 2015). Cai et al. (2016) also reported that extracts of Kunlun Chrysanthemum flower prevented high blood glucose levels, improved glucose tolerance in high-fat mice, and exhibited α-glucosidase inhibitory activity. Certain extracted components of Kunlun Chrysanthemum, including phenolic acids, chalcones, and flavonoids, inhibited NO production in N9 cells, showing anti-neuroinflammatory activity (Li et al., 2015). Moreover, Kunlun Chrysanthemum contains carbohydrates, amino acids, and flavonoids (Guo et al., 2015a). Of these, carbohydrates are considered the major biologically active components in Kunlun Chrysanthemum with pharmacological functions, including antioxidant and anti-proliferative activity (Jing et al., 2016). However, there are no studies on the effects of Kunlun Chrysanthemum oligosaccharides, in terms of anti-neuroinflammation or α-glucosidase and α-amylase inhibitory activities. Additionally, there are only a few reports on the detailed structures of purified oligosaccharides from Kunlun Chrysanthemum. In this study, we isolated, purified, and characterized three oligosaccharides from Kunlun Chrysanthemum and measured their anti-neuroinflammation activities, as well as the α-glucosidase and α-amylase inhibitory activities.

2. Materials and methods

2.1. Materials and chemicals

The flowers of Kunlun Chrysanthemum were obtained from Minfeng county, Hetian city, Xinjiang Autonomous Region, China. Voucher specimens (No. 2017061101) were deposited in the School of Pharmacy at Guangdong Pharmaceutical University. Cellulose DEAE-52 was purchased from Whatman Co. (Maidstone, Kent, U.K.). Sephacryl S-100 HR gel filtration medium was purchased from GE Healthcare Bio-Sciences AB (Uppsala, Sweden). Standard monosaccharides, T-series dextran, 1-phenyl-3-methyl-5-pyr-azolone (PMP), trifluoroacetic acid (TFA), dimethyl-sulfoxide (DMSO), and Congo red were purchased from Sigma Chemical Co. (St. Louis, MO, USA). α-Glucosidase and α-amylase were purchased from Sigma Aldrich (Steinheim, Germany). BV2 cells were purchased from the School of Basic Medical Science at Peking Union Medical College. All other chemicals and solvents were of analytical grade.

2.2. Extraction of Kunlun Chrysanthemum oligosaccharides

Twenty kilograms flowers of Kunlun Chrysanthemum were divided into two parts. Each 10 kg were extracted with distilled water 1:10 (w/v) at 80 °C for 3 h, and the extraction was repeated three times. The supernatant was concentrated to 1/7 of the initial volume under reduced pressure and was further precipitated with 95% ethanol to a final concentration of 50% over 24 h. The precipitates (P50) were collected. The supernatants were then concentrated and precipitated by 95% ethanol to a final concentration of 70% to obtain P70.

2.3. Isolation and purification of Kunlun Chrysanthemum oligosaccharides

P70 was selected for further purification based on its water-solubility and higher yield. After deproteinization and dialysis (molecular weight cut-off 1000 Da), P70 was concentrated and freeze-dried. Subsequently, P70 was dissolved in distilled water (20 mg/mL) and centrifuged (8124 g) for 5 min. The supernatants (10 mL) were separated on a DEAE-52 column (Ø 2.5 × 45 cm). The column was eluted with a gradient of NaCl solution (0–1 M) at a flow rate of 1.2 mL/min. The elution was collected via automatic fraction collector and monitored by the phenol-sulfuric acid method (Dubois et al., 1956) to obtain two fractions. The fraction eluted with distilled water, labeled as P70-1, was collected, concentrated and dialyzed with cellulose membrane (molecular weight cut-off 1000 Da) against distilled water in a 2 L beaker. The solution outside the dialysis tube was collected, concentrated, freeze-dried and further purified via Sephacryl S-100 gel-filtration column (Ø 1.6 × 100 cm), eluting with distilled water at a flow rate of 20 mL/h. Two subfractions containing carbohydrates were collected and labeled as CT70-1A and CT70-1B, respectively. Another fraction eluted with 0.015 M NaCl, labeled as P70-2, was collected, concentrated and dialyzed (molecular weight cut-off 100 Da). The solution inside the dialysis tube was collected, concentrated and freeze-dried. P70-2 (20 mg/mL) was further purified via Sephacryl S-100 gel-filtration column (Ø 1.6 × 100 cm), eluting with distilled water at a flow rate of 20 mL/h. The eluate was collected, freeze-dried, and labeled as CT70-2. The procedure of extraction and purification of three oligosaccharides from the flowers of Kunlun Chrysanthemum was shown in Scheme S1. The structures and bioactivities of CT70-1A, CT70-1B, and CT70-2 were studied in the following experiments.

2.4. Determination of homogeneity, molecular weight and optical ratation

The homogeneity of oligosaccharide was determined using specific optical rotation method (Qian et al., 2009). Eighty milligrams of oligosaccharide samples were dissolved in distilled water, and anhydrous ethanol was added to a final concentration of 70%. One precipitate was obtained after centrifugation (8124 g) for 5 min. Subsequently, anhydrous ethanol was added to the supernatant to obtain a final concentration of 80%, and another precipitate was obtained. The two precipitates were dissolved in distilled water to a final concentration of 2 mg/mL, respectively. The optical rotation of the solution was determined using a P8000 Kruss polarimeter (Germany) (Li et al., 2013).

The homogeneity and molecular weight distribution of samples were further estimated by high-performance gel permeation chromatography (HPGPC), equipped with a Waters 2414 refractive index detector and TSK-GEL G-5000PW$_{XL}$ and G-3000PW$_{XL}$ gel column in series (Tosoh Biosep, Japan) (Wang et al., 2017b). Twenty microliters of sample solution (3 mg/mL) were eluted with 0.02 M KH_2PO_4 solution at a flow rate of 0.5 mL/min. The columns were calibrated with T-series Dextran standards (Dextran T1000, T500, T70, T40, T10, and T5). The average molecular weight was estimated via the calibration curve obtained.

Matrix-assisted laser desorption/ionization time-of-flight mass spectrometry (MALDI-TOF-MS, Bruker ultraFleXtreme, Germany) was used to detect the molecular weight distribution. The sample solution

(0.5 μL) was mixed with 0.5 μL of the matrix solution, and 1 μL of the mixture was applied to a stainless steel sample slide and dried under vacuum. Mass spectra were acquired from 700 *m/z* to 3500 *m/z* in positive linear mode (Arrizon et al., 2010).

2.5. Monosaccharide component analysis of Kunlun Chrysanthemum oligosaccharides

The monosaccharide composition of oligosaccharide was determined by PMP precolumn derivatization and HPLC method (Dai et al., 2010; Wu et al., 2014). Briefly, 5 mg of each oligosaccharide was hydrolyzed by 2 M TFA (2 mL) at 90 °C in sealed tubes for 30 min, respectively. Then, the hydrolysate was co-distilled with methanol to remove excess TFA until the pH returned to neutral.

The residues of CT70-1A and CT70-1B or monosaccharides standard mixture (mannose, rhamnose, glucuronic acid, galacturonic acid, glucose, galactose, xylose, arabinose, and fucose) were further mixed with 100 μL PMP methanol solution (0.5 M). The mixture was incubated for 30 min at 70 °C and neutralized with 100 μL of 0.3 M HCl solution. The aqueous solution of derivatization was extracted with equivalent volume of chloroform and repeated for three times to remove the PMP residues. Finally, samples were filtered through a 0.45 μm filter and analyzed by an Agilent 1260 HPLC system (Agilent, Santa Clara, CA, USA). The mobile phase was 0.05 M NaH_2PO_4–Na_2HPO_4 elution buffer (pH 6.7) and acetonitrile (83:17, v/v) at a flow rate 1 mL/min. The system was coupled with a ZOR-BAX Eclipse XDB C-18 column and an ultraviolet detector (Jiang et al., 2016).

The monosaccharide composition of CT70-2 was determined by high-performance anion exchange chromatography with amperometric detection (HEPAEC-PAD) (Wang et al., 2017a). The hydrolysate residue of CT70-2 was re-dissolved in 1 mL of distilled water. The solution or monosaccharide standard mixture (mannose, rhamnose, glucose, galactose, xylose, arabinose, fructose, and fucose) was analyzed on an HPAEC-PAD coupled with a CarboPac PA10 column (250 × 2 nm), followed by elution with H_2O and 250 mM NaOH (96:4, v/v) at a flow rate 0.2 mL/min.

2.6. Fourier transform-infrared (FT-IR) spectrum analysis

Samples (1 mg) were mixed with KBr (100 mg), pressed into a pellet, and then analyzed with a PerkinElmer FT-IR spectrometer from 4000 to 400 cm^{-1}(Yan et al., 2019) .

2.7. Methylation of Kunlun Chrysanthemum oligosaccharides

The oligosaccharides were methylated according to the method reported by Huang et al. (2015). The oligosaccharide (3.5 mg) was dissolved in 1 mL anhydrous methanol and evaporated. The residue was dissolved in 5 mL DMSO and then methylated with DMSO/NaOH slurry (5 mL/40 mg) and 7.5 mL CH_3I in an ultrasonic bath to accelerate the reaction. The complete methylation was confirmed by the disappearance of the hydroxyl absorption peak in the IR spectrum. Then, the methylated sample was hydrolyzed with 2 mL TFA (3 M) for 6 h at 120 °C and dehydrated again by adding 1 mL anhydrous methanol. Later, the product was dissolved with 2 mL distilled water, reduced with 20 mg $NaBH_4$ for 30 min at 40 °C, acetylated with 100 μL acetic anhydride–pyridine (1:1 molar ratio) for 120 min at 95 °C. The final product was subjected to GC-MS (GC-MS-QP 2010; Shimadzu, Kyoto, Japan) to analyze the methylated alditol acetates. The temperature programming method was used for GC/MS assay. The temperature of column was kept at 150 °C for 1 min, and increased from 150 °C to 180 °C at a rate of 10 °C/min and maintained at 180 °C for 1 min, then up to 260 °C at a rate of 15 °C/min and kept at 260 °C for 5 min. The injection temperature was 220 °C. The mass spectra were acquired from 40 *m/z* to 400 *m/z*.

2.8. Nuclear magnetic resonance (NMR) analysis

Fifty milligrams of oligosaccharide were dissolved in 750 μL D_2O. The proton nuclear magnetic resonance (^{1}H NMR), carbon-13 nuclear magnetic resonance (^{13}C NMR) and Two-dimensional (2D) spectroscopy, including heteronuclear single-quantum coherence (HSQC) and heteronuclear multiple-bond correlation (HMBC) were obtained from a Bruker AV-500 spectrometer (Germany) with tetra-methylsilane (TMS) as the internal standard.

2.9. α-Glucosidase inhibitory activity

The α-glucosidase inhibitory activity was determined according to a previously published method (Striegel et al., 2015). A mixture of 40 μL sample (dissolved in 0.1 M phosphate buffer), 20 μL α-glucosidase (0.2 U/mL), and 0.1 M phosphate buffer (pH 6.8, 50 μL) were incubated in 96-well plates at 37 °C for 5 min. Then, 50 μL of 10 mM *p*-nitrophenyl-α-D-glucopyranoside solution dissolved in 0.1 M phosphate buffer (pH 6.8) were added to each well. The reaction mixtures were incubated at 37 °C for 30 min. The catalytic reaction was terminated by the addition of 1 mL Na_2CO_3 solution (0.1 M). Acarbose served as the positive control. The reaction system without saccharides was used as the blank. The absorbance was measured at 405 nm with a UV–Vis spectrophotometer, and the inhibition percentage was expressed as follows:

$$\text{Inhibition percentage } (\%) = \frac{A_{blank} - A_{sample}}{A_{blank}} \times 100\% \quad (1)$$

2.10. α-Amylase inhibitory activity

The α-amylase inhibitory activity was determined according to the literature (Eleazu et al., 2016). Twenty-five microliters of sodium phosphate buffer (20 mM, pH 6.8), 25 μL sample solution (dissolved in 20 mM sodium phosphate buffer), and 0.5 mg/mL α-amylase (dissolved in 20 mM sodium phosphate buffer) were mixed in a microcentrifuge tube. The mixture was incubated for 10 min at 25 °C. Then, 25 μL of 0.5% starch solution in sodium phosphate buffer (20 mM, pH 6.8) was added. The reaction mixture was kept at 25 °C for 10 min. Next, 50 μL of 96 mM 3,5-dinitrosalicylic acid were added and heated in boiling water for 5 min. The mixture was then cooled to room temperature. Acarbose was used as the positive control. The reaction system without saccharides was used as the blank. The absorbance was measured at 540 nm with a UV–Vis spectrophotometer, and the inhibition percentage was calculated.

2.11. Effects of Kunlun Chrysanthemum saccharides on the viability and NO production of BV2 cells

The viability of BV2 cells was examined by MTT method. BV2 cells were maintained in DMEM medium supplemented with 10% fetal bovine serum (FBS), 100 units/mL penicillin and 100 μg/mL streptomycin. All cells were cultured in a humidified atmosphere containing 5% CO_2 at 37 °C. BV2 cells were seeded into a 96-well plate with a density of 3 × 10^4 cells/mL and cultured for 24 h. After being treated with tested samples (10 μL) for 24 h, the BV2 cells were incubated with 20 μL MTT (5 mg/mL) for 4 h. Then, 150 μL of DMSO were added to each well, and the absorbance was measured on a microplate reader at 490 nm.

The NO production of BV2 cells was determined according to a previously published method (Nhiem et al., 2017). BV2 cells were seeded into a 96-well plate with a density of 3 × 10^5 cells/mL and incubated at 37 °C and 5% CO_2 for 24 h. BV2 cells were treated with different concentrations of P70 (30, 60, 120, 240 μg/mL), CT70-1A, CT70-1B, CT70-2 (12.5, 25, 50, 100, 200 μM), or indomethacin (12.5, 25, 50, 100 μM) for 48 h at 37 °C in the presence of LPS (1 μg/mL). Fifty

microliters of the cell supernatant were mixed with the I and II solutions from the NO kits. The absorbance was measured on a microplate reader at 540 nm. The percentage of NO inhibition was calculated as follows:

$$\text{Inhibition percentage } (\%) = (A_l - A_s)/(A_l - A_c) \times 100\%, \quad (2)$$

where A_c is the absorbance of the control group (the reaction system without sample or LPS); A_s is the absorbance of the sample group; and A_l is the absorbance of the LPS group (the reaction system without sample).

2.12. Statistical analysis

Results are expressed as mean ± SD. Statistical analysis of experimental data was performed using one-way analysis of variance (one-way ANOVA) for at least three independent biological replicates. All calculations were performed using Graph Pad Prism6 (GraphPad Software, San Diego, CA). $P < 0.05$ was considered statistically significant.

3. Results and discussion

3.1. Basic properties of Kunlun Chrysanthemum oligosaccharides

Crude saccharides were isolated from Kunlun Chrysanthemum through hot water extraction, ethanol precipitation, and deproteinization. P70 was separated on a DEAE-cellulose 52 column and eluted with distilled water and 0.015 M NaCl to gain P70-1 and P70-2, respectively. P70-1 was dialyzed with a cellulose membrane (molecular weight cut-off, 100 Da) and subsequently purified by using a Sephacryl S-100 column. Distilled water was used as the eluent to obtain CT70-1A and CT70-1B. After dialysis, P70-2 was further purified by a Sephacryl S-100 column and eluted with distilled water to obtain CT70-2.

CT70-1A, CT70-1B and CT70-2 all showed a single symmetrical peak by HPGPC detection (Fig. 1 and Figs. S1–S2), indicating that they were all homogeneous oligosaccharides, and their molecular weights were 1221, 1318, and 1247 Da, respectively. The differentials of specific optical rotation were no more than 5° between the two fractional precipitates, further indicating that each sample was a homogeneous oligosaccharide, which were consistent with the results of HPGPC. Their specific optical rotations were = -9°, −37°, and −20°, respectively.

3.2. Monosaccharide composition analysis of Kunlun Chrysanthemum oligosaccharides

As shown in Fig. 2 and Figs. S3–S4, the results of HPLC and HPAEC-PAD revealed that CT70-1A, CT70-1B, and CT70-2 were all composed of mannose, glucose, galactose, and arabinose.

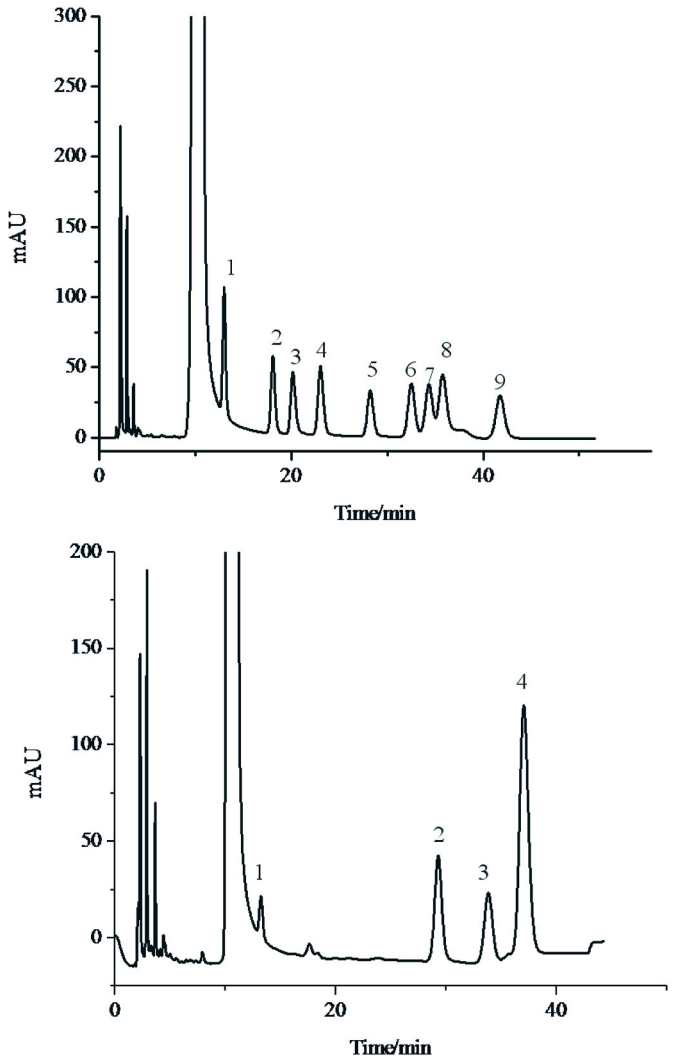

Fig. 2. HPLC analysis of the mixture of standard monosaccharides (A) and component monosaccharides of CT70-1A (B). 1, mannose; 2, rhamnose; 3, glucuronic acid; 4, galacturonic acid; 5, glucose; 6, galactose; 7, xylose; 8, arabinose; 9, fucose.

3.3. FT-IR analysis of Kunlun Chrysanthemum oligosaccharides

The IR spectra of Kunlun Chrysanthemum oligosaccharides are shown in Fig. 3 and Figs. S5–S6. A broad bands at 3349 cm^{-1} (CT70-1A),

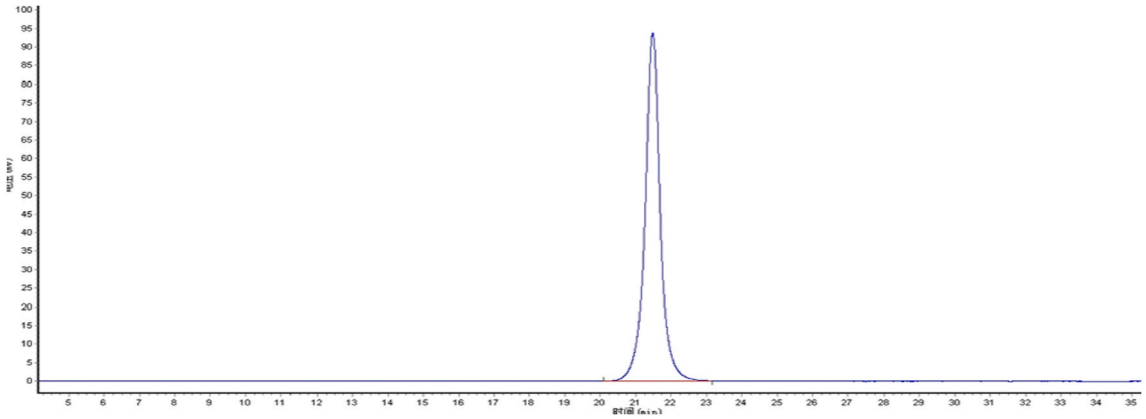

Fig. 1. The HPGPC chromatogram of CT70-1A.

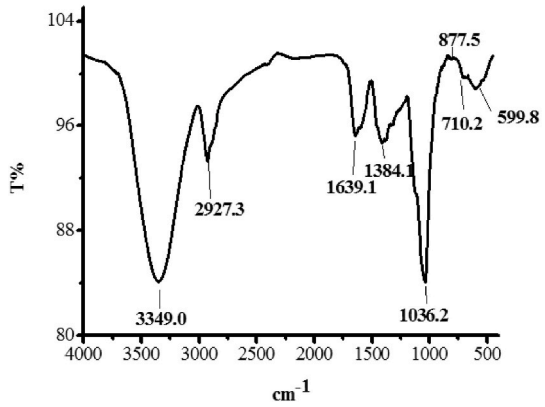

Fig. 3. IR spectrum of CT70-1A.

3358 cm^{-1} (CT70-1B), and 3393 cm^{-1} (CT70-2) were matched the hydroxyl stretching vibration of oligosaccharides. The peaks around 2927 cm^{-1} (CT70-1A), 2933 cm^{-1} (CT70-1B), and 2927 cm^{-1} (CT70-2) were corresponded to the C–H stretching vibration. A weak bands appeared at 1639 cm^{-1}(CT70-1A), 1643 cm^{-1} (CT70-1B), and 1638 cm^{-1} (CT70-2) were due to absorption of water, because of hygroscopic properties of this oligosaccharide. The bands around 1036 cm^{-1}(CT70-1A), 1026 cm^{-1} (CT70-1B), and 1035 cm^{-1} (CT70-2) were the characteristic peaks of pyranose configuration of the oligosaccharides. In addition, the peak at 938 cm^{-1} indicated the existence of the furan ring in CT70-2 (Wang et al., 2017a; Albuquerque et al., 2014).

3.4. Methylation and GC-MS analysis

GC-MS analysis was performed to identify linkages in the sugar residue. The methylated oligosaccharides were acid hydrolyzed and acetylated prior to GC-MS analysis. Mass spectrum of methylated sugar residues are shown in Figs. S7–S9. The results of methylation analysis by GC-MS are shown in Table 1 and Tables S1–S2. Five residues of CT70-1A were identified, including 1,5-di-*O*-acetyl-2,3,4,6-tetra-*O*-methyl-D-glucitol, 1,2,4-tri-*O*-acetyl-3,5-di-*O*-methyl-L-arabinitol, 1,5,6-tri-*O*-acetyl-2,3,4-tri-*O*-methyl-D-galactitol, 1,3,5,6-tetra-*O*-acetyl-2,4-di-*O*-methyl-D-mannitol, and 1,5,6-tri-*O*-acetyl-2,3,4-tri-*O*-methyl-D-glucitol. These results indicate that CT70-1A may be composed of Glc*p*-(1→, →2)-Ara*f*-(1→, →6)-Gal*p*-(1→, →3,6)-Man*p*-(1→ and →6)-Glc*p*-(1→ at a ratio of 11.34:4.21:3.05:4.93:4.01, respectively, which was about 3:1:1:1:1. That also indicated the three terminal Glc were coincident.

Table 1
GC-MS data of the methylated products of CT70-1A.

PMAA	Molar ratio	Mass fragments (m/z)	Linkage
1,5-di-*O*-acetyl-2,3,4,6-tetra-*O*-methyl-D-glucitol	11.34	43,57,71,87,101,118,129,145,162	Glc*p*-(1→
1,2,4-tri-*O*-acetyl-3,5-di-*O*-methyl-L-arabinitol	4.21	43,57,87,101,111,129,146,161	→2)-Ara*f*-(1→
1,5,6-tri-*O*-acetyl-2,3,4-tri-*O*-methyl-D-galactitol	3.05	43,57,87,99,101,117,129,169,189	→6)-Gal*p*-(1→
1,3,5,6-tetra-*O*-acetyl-2,4-di-*O*-methyl-D-mannitol	4.93	43,57,87,101,117,129,139,189,234	→3,6)-Man*p*-(1→
1,5,6-tri-*O*-acetyl-2,3,4-tri-*O*-methyl-D-glucitol	4.01	43,57,71,99,101,117,129,143,161,173	→6)-Glc*p*-(1→

Six residues of CT70-1B were present, including 1,5-di-*O*-acetyl-2,3,4,6-tetra-*O*-methyl-D-glucitol, 1,2,3,5,6-penta-*O*-acetyl-4-*O*-methyl-D-glucitol, 1,2,4-tri-*O*-acetyl-3,5-di-*O*-methyl-L-arabinitol, 1,5,6-tri-*O*-acetyl-2,3,4-tri-*O*-methyl-D-galactitol, 1,3,5,6-tetra-*O*-acetyl-2,4-di-*O*-methyl-D-mannitol, and 1,4-di-*O*-acetyl-2,3,5-tri-*O*-methyl-L-arabinitol. These results indicate that the main residue linkages of CT70-1B were Glc*p*-(1→, →2,3,6)-Glc*p*-(1→, →2)-Ara*f*-(1→, →6)-Gal*p*-(1→, →3,6)-Man*p*-(1→ and Ara*f*-(1 → .

Five residues of CT70-2 were identified, including 1,5-di-*O*-acetyl-2,3,4,6-tetra-*O*-methyl-D-glucitol, 1,4,5-tri-*O*-acethyl-2,3,6-tri-*O*-methyl-D-glucitol, 1,4-di-*O*-acetyl-2,3,5-tri-*O*-methyl-L-arabinitol, 1,5,6-tri-*O*-acetyl-2,3,4-tri-*O*-methyl-D-galactitol and 1,3,5,6-tetra-*O*-acetyl-2,4-di-*O*-methyl-D-mannitol. These results indicate that the main residue linkages of CT70-2 were Glc*p*-(1→, →4)-Glc*p*-(1→, Ara*f*-(1→, →6)-Gal*p*-(1→ and →3,6)-Man*p*-(1 → .

3.5. NMR spectra of Kunlun Chrysanthemum oligosaccharides

The ^{1}H and ^{13}C NMR spectra of CT70-1A are shown in Fig. 4. In the ^{1}H NMR spectrum, all chemical signals were distributed from 1.00 to 6.00 ppm. Those in the range of 4.00–6.00 ppm were associated with anomeric protons. The α and β configurations of the residues were determined via the chemical shift and coupling constants of the anomeric proton (Habibi et al., 2004). The ^{1}H NMR data showed signals at δ_H 4.41, 4.83, 5.04, and 5.36 ppm, which were attributed to characteristic anomeric proton signals. An examination of the ^{13}C NMR data disclosed five anomeric carbon signals at δ_C 92.4, 100.1, 102.2, 103.1, and 108.3 ppm, which substantiated that there were five residues in CT70-1A. The result was consistent with the result of GC-MS. In the HSQC spectra (Fig. 4C), we observed the correlations of 5.36 with 92.4, 5.36 with 108.3, 5.04 with 102.2, 4.83 with 100.1, and 4.41 with 103.1. Comprehensive analyses of ^{1}H NMR, ^{13}C NMR, HSQC spectra and GC-MC suggested that the glycosidic linkages were followed by (1→)-linked α-D-glucose, (1 → 2)-linked α-L-arabinose, (1 → 6)-linked β-D-galactose, (1 → 6)-linked α-D-glucose and (1 → 3, 6)-linked β-D-mannose (Dertli et al., 2017; Sahragard and Jahanbin, 2017; Zhao et al., 2017; Li et al., 2017). Furthermore, based on the correlations of HMBC spectrum, the H2/C2, H3/C3, H4/C4, H5/C5, and H6/C6 chemical shifts of each residue were defined. Thus, the combined ^{1}H, ^{13}C, HSQC, and methylation data, along with data from the literature (Wang et al., 2009; Westphal et al., 2010; Pattanayak et al., 2015; Guo et al., 2015b), led to complete descriptions of the residues of CT70-1A (Table 2).

The HMBC spectra showed cross-peaks in different residues, confirming the linkage sites and sequences among residues. Fig. 4D shows cross-peaks that could be assigned as follows: H1 (5.36 ppm) of residue A and C2 (84.0 ppm) of residue B (AH1/BC2), suggesting that the C-2 of residue B was linked to the O-1 of residue A. The cross-peaks of 4.03/108.3 ppm (DH3/BC1), 3.45/102.2 ppm (DH6/EC1), 5.36/72.3 ppm (AH1/FC6), 4.83/72.1 ppm (FH1/EC6), and 5.36/103.1 ppm (AH1/DC1) suggest that the C-1 of residue B was linked to the O-3 of residue D, the C-1 of residue E was linked to the O-6 of residue D, the C-6 of residue F was linked to the O-1 of residue A, the C-6 of residue E was linked to the O-1 of residue F, and the C-1 of residue D was linked to the O-1 of residue A.

The ^{1}H and ^{13}C NMR spectra of CT70-1B are shown in Fig. S10. The ^{1}H NMR data show the characteristic anomeric proton signals at δ_H 4.41, 4.36, 4.84, 5.16, and 5.36 ppm. An examination of the ^{13}C NMR data disclosed six anomeric carbon signals at δ_C 92.4, 99.7, 103.0, 103.2, 108.6, and 109.4 ppm, which indicated that there were six residues in CT70-1B. The result was consistent with the result of GC-MS. In the HSQC spectra (Fig. S10C), we observed the correlations of 5.36 with 92.4, 5.36 with 108.6, 5.16 with 109.4, 4.84 with 99.7, 4.41 with 103.0 and 4.36 with 103.2. A comprehensive analysis of ^{1}H NMR, ^{13}C NMR, HSQC spectra, and GC-MC suggested that the glycosidic linkages were

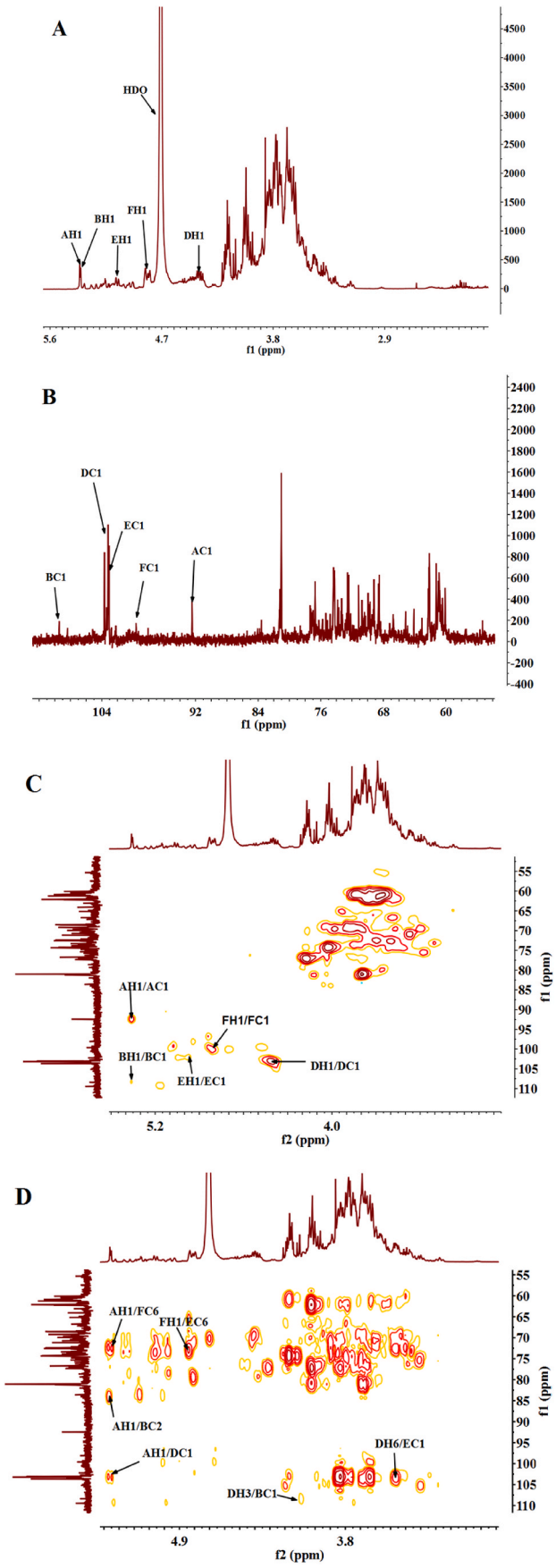

Fig. 4. ^{1}H (A), ^{13}C (B), HSQC (C), and HMBC (D) spectra of CT70-1A.

Table 2
Chemical shifts for the resonances of glycosyl residues in CT70-1A, obtained from ^{1}H and^{13}C NMR spectra.

Sugar residue	C1/ H1	C2/ H2	C3/ H3	C4/ H4	C5/ H5	C6/H6
α-D-Glc*p*-(1→	92.4	72.3	75.1	73.1	75.3	65.1
A	5.36	3.70	3.87	3.30	3.83	3.72/ 3.93
→2)-*α*-L-Ara*f*-(1→	108.3	84.0	79.3	80.7	67.2	–
B	5.36	4.01	4.19	4.37	3.96	–
→3,6)-*β*-D-Man*p*-(1→	103.1	72.0	79.3	75.1	72.6	67.2
D	4.41	3.98	4.03	3.87	3.60	3.45
→6)-*β*-D-Gal*p*-(1→	102.2	74.2	74.3	73.6	77.1	72.1
E	5.04	4.03	4.18	3.85	4.17	4.15
→6)-*α*-D-Glc*p*-(1→	100.1	76.8	76.6	75.1	75.6	72.3
F	4.83	4.03	3.85	3.75	3.38	3.70/ 3.64

followed by (1→)-linked *α*-D-glucose, (1 → 2)-linked *α*-L-arabinose, (1→)-linked *α*-L-arabinose, (1 → 2,3,6)-linked *α*-D-glucose, (1 → 6)-linked *β*-D-galactose, and (1 → 3, 6)-linked *β*-D-mannose (Dertli et al., 2017; Sahragard and Jahanbin, 2017; Zhao et al., 2017; Li et al., 2017). Furthermore, based on the correlations of the HMBC spectrum, the H2/C2, H3/C3, H4/C4, H5/C5, and H6/C6 chemical shifts of each residue were defined. Thus, based on the ^{1}H, ^{13}C, HSQC, and methylation data, and in combination with data published from related studies (Wang et al., 2009; Westphal et al., 2010; Pattanayak et al., 2015; Guo et al., 2015b), we assigned a complete description of the residues of CT70-1B (Table S3).

The HMBC spectra showed cross-peaks in different residues, confirming the linkage sites and sequences among residues. Fig. S10D shows cross-peaks that could be assigned as follows: H1 (5.36 ppm) of residue A and C2 (84.1 ppm) of residue F (AH1/FC2), suggesting that the C-2 of residue F was linked to the O-1 of residue A. The cross-peaks of 4.08/108.6 ppm (BH3/FC1), 5.36/80.4 ppm (AH1/EC3), 3.94/109.4 ppm (BH2/GC1), 3.68/109.4 ppm (EH6/GC1), 3.86/103.0 ppm (BH6/EC1), 5.36/103.2 ppm (AH1/DC1), and 4.84/72.6 ppm (BH1/DC6) suggest that the C-1 of residue F was linked to the O-3 of residue B, the C-3 of residue E was linked to the O-1 of residue A, the C-1 of residue G was linked to the O-2 of residue B, the C-1 of residue G was linked to the O-6 of residue E, the C-1 of residue E was linked to the O-6 of residue B, the C-1 of residue D was linked to the O-1 of residue A, and the C-6 of residue D was linked to the O-1 of residue B.

The ^{1}H and ^{13}C NMR spectra of CT70-2 are shown in Fig. S11. The ^{1}H NMR data showed characteristic anomeric proton signals at δ_H 4.41, 5.02, 5.10, 5.18 and 5.36 ppm. Examination of the ^{13}C NMR data disclosed five anomeric carbon signals at δ_C 92.4, 99.9, 103.3, 107.4 and 109.2 ppm, indicating the presence of five residues in CT70-2. The result was consistent with the result of GC-MS. In the HSQC spectra (Fig. S11C), we observed the correlations of 5.36 with 92.4, 5.18 with 109.2, 5.10 with 99.9, 5.02 with 107.4 and 4.41 with 103.3. Comprehensive analyses of ^{1}H NMR,^{13}C NMR, HSQC spectra and GC-MC suggested that the glycosidic linkages were followed by (1→)-linked *α*-D-glucose, (1→)-linked *α*-L-arabinose, (1 → 4)-linked *α*-D-glucose, (1 → 6)-linked *β*-D-galactose, and (1 → 3, 6)-linked *β*-D-mannose (Dertli et al., 2017; Sahragard and Jahanbin, 2017; Zhao et al., 2017; Li et al., 2017). Furthermore, based on the correlations of HMBC spectrum, the H2/C2, H3/C3, H4/C4, H5/C5 and H6/C6 chemical shifts of each residue were defined. Thus, combined with the ^{1}H, ^{13}C, HSQC, and methylation data as well as the related references (Wang et al., 2009; Westphal et al., 2010; Pattanayak et al., 2015; Guo et al., 2015b), we assigned a complete description of residues of CT70-2 (Table S4).

The HMBC spectra showed cross-peaks in different residues, confirming the linkage sites and sequences among residues. Fig. S11D shows cross-peaks that could be assigned as follows: H1 (5.36 ppm) of residue A and C6 (72.4 ppm) of residue D (AH1/DC6), suggesting that the C-6 of

residue D was linked to the O-1 of residue A. The cross-peaks of 3.83/109.2 ppm (BH4/EC1), 5.10/81.1 ppm (BH1/FC3), 3.64/107.4 ppm (FH6/DC1), and 5.36/103.3 ppm (AH1/FC1) indicate that the C-1 of residue E was linked to the O-4 of residue B, the C-3 of residue F was linked to the O-1 of residue B, the C-1 of residue D was linked to the O-6 of residue F, and the C-1 of residue F was linked to the O-1 of residue A. In addition, the 3.83/99.9 ppm (BH4/BC1) cross-peaks suggested that C-1 of residue B was linked to the O-4 of residue B, indicating that residue B was repeated in CT70-2.

In summary, the predicted structures of CT70-1A, CT70-1B and CT70-2 were shown in Scheme 1. The three oligosaccharides were composed of glucose, mannose, galactose, and arabinose in different ratios. Interestingly, they were all composed of (1 → 6)-linked *β*-D-Gal*p*, (1 → 3, 6)-linked *β*-D-Man*p* and *α*-D-Glc*p*-(1 → . However, there were also some different residues in them. CT70-1A also consisted of (1 → 2)-linked *α*-L-Ara*f* and (1 → 6)-linked *α*-D-Glc*p*. CT70-1B also included (1 → 2)-linked *α*-L-Ara*f*, (1 → 2,3,6)-linked *α*-D-Glc*p* and *α*-L-Ara*f*-(1 → . And CT70-2 also consisted of (1 → 4)-linked *α*-D-Glc*p* and *α*-L-Ara*f*-(1 → . In short, CT70-1A, CT70-1B and CT70-2 were all novel oligosaccharides.

3.6. *α*-Glucosidase inhibitory activity of Kunlun Chrysanthemum saccharides

The inhibition of *α*-glucosidase, a key carbohydrate hydrolyzing enzyme, could serve as a promising target for the treatment of diabetes by controlling the postprandial glucose levels and suppressing postprandial hyperglycemia (Ademiluyi et al., 2014). The *α*-glucosidase inhibitory activities of Kunlun Chrysanthemum saccharides are presented in Fig. 5. P70 is a crude saccharide obtained from Kunlun Chrysanthemum. P70 was deproteinized to get the saccharide dP70. P70 and dP70 had almost the same effects on *α*-glucosidase inhibitory activity, revealing that the protein was not the bioactive component in crude saccharide P70. CT70-1A mildly inhibited *α*-glucosidase, with an IC_{50} value of 2.68 ± 0.10 mM (3.27 ± 0.01 mg), while CT70-1B and CT70-2 had IC_{50} values of 2.62 ± 0.06 mM (3.45 ± 0.08 mg) and 4.89 ± 0.02 mM (6.05 ± 0.02 mg), respectively. CT70-1B, CT70-2, and CT70-1A had better *α*-glucosidase inhibitory activities than some reported polysaccharides, such as PRM3 isolated from the *Rhynchosia minima* root (IC_{50} value of 8.85 mg/mL) (Jia et al., 2017). The result suggested that Kunlun Chrysanthemum oligosaccharides may be the active components responsible for the anti-diabetic activities of Kunlun Chrysanthemum.

3.7. *α*-Amylase inhibitory activity of Kunlun Chrysanthemum saccharides

α-Amylase is one of the major secretory products of the pancreas and salivary glands, and plays a role in the digestion of starch and glycogen. The inhibition of *α*-amylase can control the breakdown of dietary starch into smaller oligomers to delay glucose absorption, which is an important aspect in the management of type 2 diabetes (Lordan et al., 2013). The *α*-amylase inhibitory activity of Kunlun Chrysanthemum saccharides is presented in Fig. 6. P70 and dP70 had similar effects on the *α*-amylase inhibitory activity, revealing the protein was not the bioactive component in crude saccharides P70. CT70-1A significantly inhibited *α*-amylase, with an IC_{50} value of 2.77 ± 0.10 mM (3.38 ± 0.01 mg), while CT70-1B and CT70-2 had IC_{50} values of 2.75 ± 0.06 mM (3.62 ± 0.08 mg) and 3.35 ± 0.03 mM (4.18 ± 0.04 mg), respectively. These values were better than that of corn silk polysaccharide N-CSPS (IC_{50} value was 10.07 mg/mL) (Chen et al., 2013).

3.8. Effects of Kunlun Chrysanthemum saccharides on the viability and NO production of BV2 cells

We determined the cytotoxicity of CT70-1A, CT70-1B, CT70-2 via NO production of BV2 cells. As shown in Fig. 7A, 240 μg/mL of Kunlun

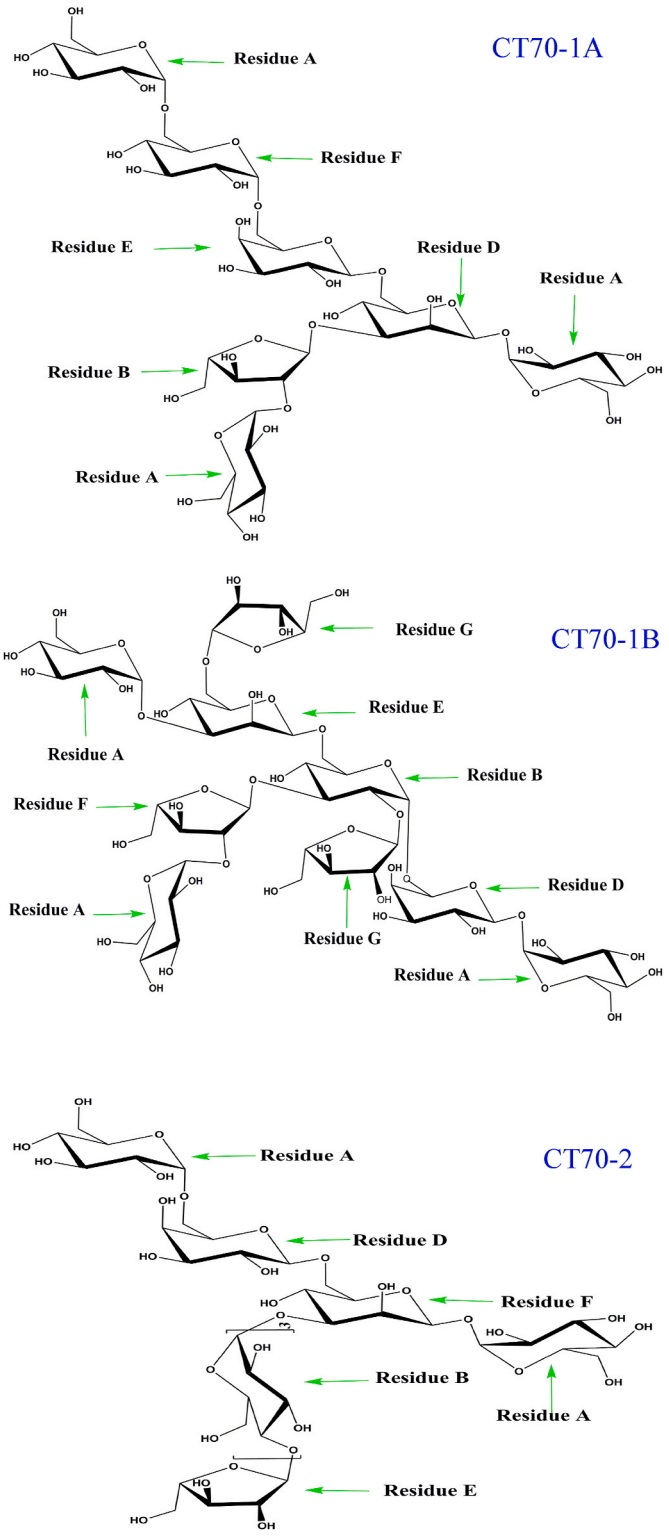

Scheme 1. The predicted structures of CT70-1A, CT70-1B and CT70-2.

Chrysanthemum crude saccharides P70 and 200 μM of homogeneous saccharides had no cytotoxic effects on BV2 cells. The result indicated that 0–240 μg/mL of crude saccharides and 0–200 μM of homogeneous saccharides could be selected as the tested concentration in the following experiment.

Extensive pathology studies revealed that AD is closely related to neuroinflammation. In the occurrence and progress of neuroinflammation, excessive amounts of NO in the central nervous system

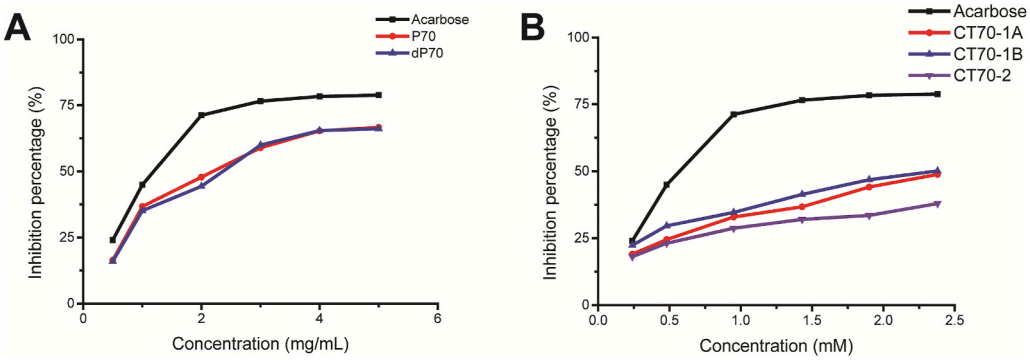

Fig. 5. α-Glucosidase inhibitory activity of Kunlun Chrysanthemum saccharides. (A) P70: Kunlun Chrysanthemum crude saccharide; dP70: the crude saccharide after deproteinization of P70; (B) CT70-1A, CT70-1B, CT70-2: the homogeneous saccharides of Kunlun Chrysanthemum.

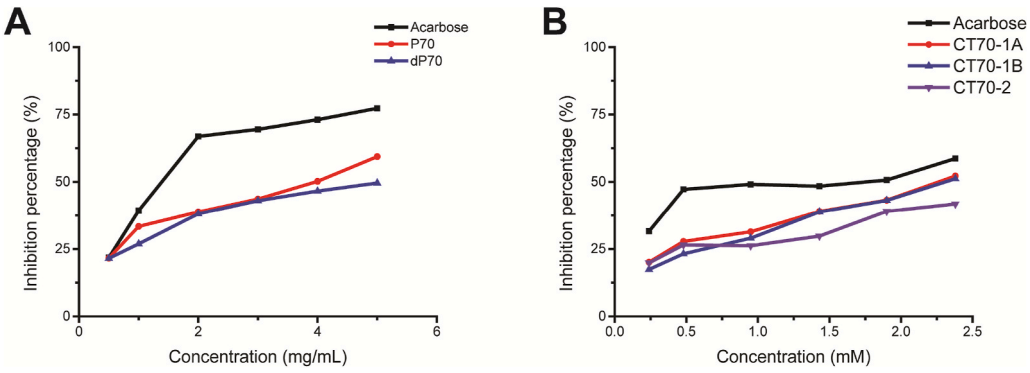

Fig. 6. α-Amylase inhibitory activity of Kunlun Chrysanthemum saccharide. (A) P70: Kunlun Chrysanthemum crude saccharide; dP70: the crude saccharide after deproteinization of P70; (B) CT70-1A, CT70-1B, CT70-2: the homogeneous saccharides of Kunlun Chrysanthemum.

(CNS) were released to stimulate microglia activation and inflammatory response, and related studies revealed that compounds with NO inhibitory effects are potentially useful for the treatment of inflammatory and related neurodegenerative diseases (Liu et al., 2018). The anti-neuroinflammatory activities of Kunlun Chrysanthemum saccharides were tested by measuring NO production in BV2 cells induced by LPS. As shown in Fig. 7B–C, the Kunlun Chrysanthemum crude saccharides P70 moderately inhibited the NO production in BV2 cells. Moreover, CT70-1A, CT70-1B and CT70-2 showed significant NO production inhibitory activities, with IC_{50} values of 0.23, 0.24 and 0.27 mM, respectively. The three purified oligosaccharides obtained from P70 exhibited synergistic effects to inhibit NO production in BV2 cells. The results suggest that CT70-1A, CT70-1B and CT70-2 are the active components in Kunlun Chrysanthemum that can be used for the treatment of AD.

4. Conclusions

In this study, we presented the characterization of three new oligosaccharides, CT70-1A, CT70-1B, and CT70-2, which were isolated from the flowers of Kunlun Chrysanthemum. Their molecular weights were 1221 Da, 1318 Da and 1247 Da, respectively. CT70-1A consisted of (1 → 2)-linked α-L-Ara*f*, (1 → 6)-linked β-D-Gal*p*, (1 → 6)-linked α-D-Glc*p*, (1 → 3, 6)-linked β-D-Man*p* and was terminated with α-D-Glc*p*-(1 → . CT70-1B consisted of (1 → 2)-linked α-L-Ara*f*, (1 → 2,3,6)-linked α-D-Glc*p*, (1 → 6)-linked β-D-Gal*p*, (1 → 3, 6)-linked β-D-Man*p* and was terminated with α-D-Glc*p*-(1→ and α-L-Ara*f*-(1 → . CT70-2 consisted of (1 → 4)-linked α-D-Glc*p*, (1 → 6)-linked β-D-Gal*p*, and (1 → 3, 6)-linked β-D-Man*p*, and was terminated with α-D-Glc*p*-(1→ and α-L-Ara*f*-(1 → . According to the rules of International Union of Pure and Applied Chemistry (1979), the systematic names of three oligosaccharides were α-D-Glc*p*1-6α-D-Glc*p*1-6β-D-Gal*p*1-6(α-D-Glc*p*1-2α-L-Ara*f*1-3)β-D-Man*p* 1-1α-D-Glc*p*, α-D-Glc*p*1-3(α-L-Ara*f*1-6)β-D-Man*p*1-6(α-D-Glc*p*1-2α-L-Ara*f*1-3)(α-L-Ara*f*1-2)α-D-Glc*p*1-6β-D-Gal*p*1-1α-D-Glc*p*, and α-D-Glc*p* 1-6β-D-Gal*p*1-6(α-L-Ara*f*1-[4α-D-Glc*p*1]$_3$-3)β-D-Man*p*1-1α-D-Glc*p*, respectively. Kunlun Chrysanthemum oligosaccharides CT70-1A, CT70-1B, and CT70-2 exhibited concentration-dependent α-glucosidase inhibitory activities, with IC_{50} values of 2.68 ± 0.10 mM, 2.62 ± 0.06 mM, and 4.89 ± 0.02 mM, respectively. The oligosaccharides also exhibited α-amylase inhibitory activities, with IC_{50} values of 2.77 ± 0.10 mM, 2.75 ± 0.06 mM, and 3.35 ± 0.03 mM, respectively. Moreover, CT70-1A, CT70-1B, and CT70-2 showed NO production inhibitory activities, with IC_{50} values of 0.23 mM, 0.24 mM and 0.27 mM, respectively. The above results suggest that Kunlun Chrysanthemum oligosaccharides are the active components responsible for the anti-diabetic effects through α-glucosidase and α-amylase inhibitory activities, and the oligosaccharides exhibit anti-neuroinflammatory effects via the inhibition of NO production. Therefore, Kunlun Chrysanthemum oligosaccharides could prevent the development of diseases such as type 2 diabetes and Alzheimer's disease, and further studies are worthy to investigate the relative pharmacological mechanism.

CRediT authorship contribution statement

Qian Yu: Writing - original draft, preparation, Writing - review & editing, Validation, Supervision. **Wei Chen:** Methodology, Development or design of methodology, Data curation, Writing - original draft, preparation. **Jing Zhong:** Investigation. **Degang Qing:** Validation. **Chunyan Yan:** Ideas, Supervision, Writing - review & editing, Funding acquisition.

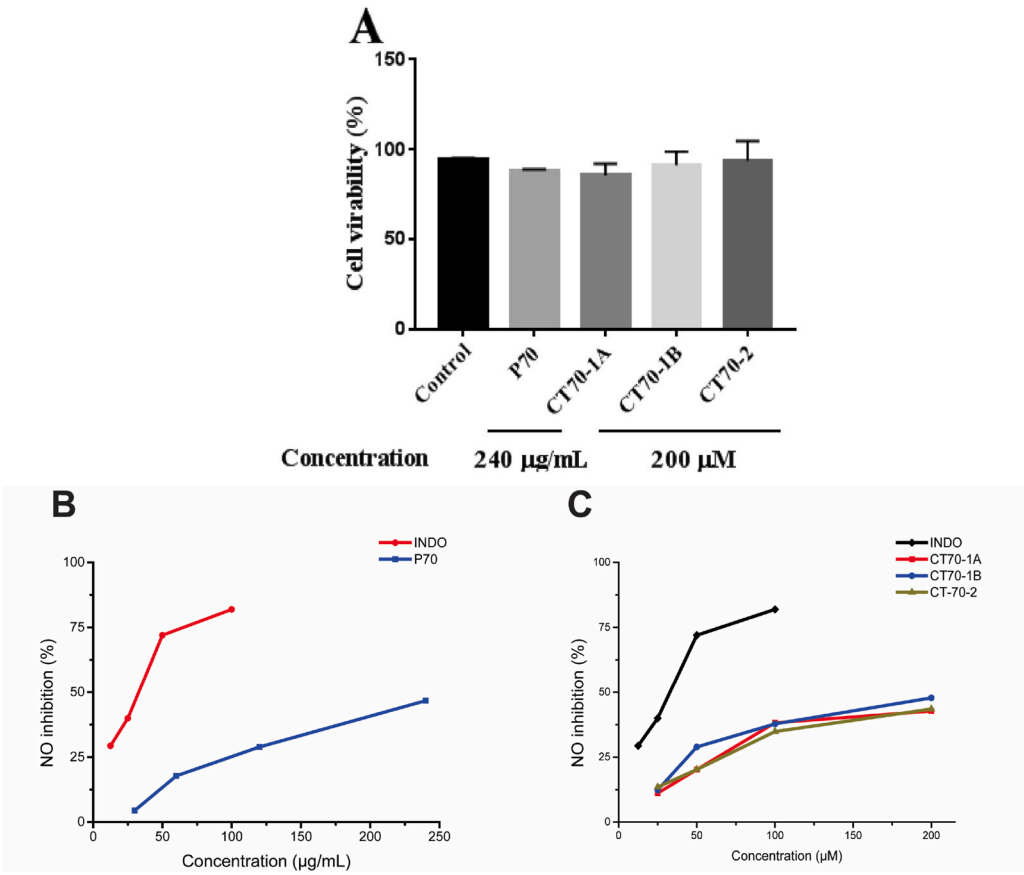

Fig. 7. The effects of Kunlun Chrysanthemum saccharides on the viability of BV2 cells (A). The effects of Kunlun Chrysanthemum saccharides on NO production of BV2 cells induced by LPS (B and C).

Declaration of competing interest

The authors declare that they have no known competing financial interests or personal relationships that could have appeared to influence the work reported in this paper.

Acknowledgments

This study was funded by the National Natural Science Foundation of China (Nos. U1703110, 81673557 and 81973454).

Appendix A. Supplementary data

Supplementary data to this article can be found online at https://doi.org/10.1016/j.fct.2021.112032.

References

Ademiluyi, A.O., Oboh, G., Boligon, A.A., Athayde, M.L., 2014. Effect of fermented soybean condiment supplemented diet on α-amylase and α-glucosidase activities in streptozotocin-induced diabetic rats. J. Funct. Foods. 9, 1–9.

Albuquerque, P.B.S., Jr, W.B., Santos, G.R.C., Correia, M.T.S., Mourão, P.A.S., Teixeira, J. A., Carneiro-da-Cunha, M.G., 2014. Characterization and rheological study of the galactomannan extracted from seeds of *Cassia grandis*. Carbohydr. Polym. 104, 127–134.

Arrizon, J., Morel, S., Gschaedler, A., Monsan, P., 2010. Comparison of the water-soluble carbohydrate composition and fructan structures of *Agave tequilana* plants of different ages. Food Chem. 122, 123–130.

Barnes, D.E., Yaffe, K., 2011. The projected impact of risk factor reduction on Alzheimer's disease prevalence. Alzheimers Dement 7, 819–828.

Cai, W., Yu, L., Yu, Z., Li, F., Kong, S., Tan, H., Xu, H., Huang, C., 2016. Extracts of *Coreopsis tinctoria* Nutt. flower exhibit antidiabetic effects via the inhibition of α-glucosidase activity. J. Diabetes Res. 23, 1–9.

Campbell, R.K., 2011. Clarifying the role of incretin-based therapies in the treatment of type 2 diabetes mellitus. Clin. Therapeut. 33, 511–527.

Chen, S., Chen, H., Tian, J., Wang, Y., Xing, L., Wang, J., 2013. Chemical modification, antioxidant and α-amylase inhibitory activities of corn silk polysaccharides. Carbohydr. Polym. 98, 428–437.

Dai, J., Wu, Y., Chen, S.W., Zhu, S., Yin, H.P., Wang, M., Tang, G., 2010. Sugar compositional determination of polysaccharides from *Dunaliella salina* by modified RP-HPLC method of precolumn derivatization with 1-phenyl-3-methyl-5-pyrazolone. Carbohydr. Polym. 82, 629–635.

Dertli, E., Colquhoun, I.J., Côté, G.L., Gall, G.L., Narbad, A., 2017. Structural analysis of the α-D-glucan produced by the sourdough isolate *lactobacillus brevis* E25. Food Chem. 242, 45–52.

Dias, T., Bronze, M.R., Houghton, P.J., Mota-Filipe, H., Paulo, A., 2010. The flavonoid-rich fraction of *Coreopsis tinctoria* promotes glucose tolerance regain through pancreatic function recovery in streptozotocin-induced glucose-intolerant rats. J. Ethnopharmacol. 132, 483–490.

Dubois, M., Gilles, K.A., Hamilton, J.K., Rebers, P.A., Smith, F., 1956. Colorimetric method for determination of sugars and related substances. Anal. Chem. 28, 350–356.

Eleazu, C.O., Eleazu, K.C., Iroaganachi, M., 2016. *In vitro* starch digestibility, α-amylase and α-glucosidase inhibitory capacities of raw and processed forms of three varieties of Livingstone potato (*Plectranthus esculentus*). Innov. Food Sci. Emerg. 37, 37–43.

Fang, Y., Xia, W., Cheng, B., Hua, P., Zhou, H., Gu, Q., Xu, J., 2018. Design, synthesis, and biological evaluation of compounds with a new scaffold as anti-neuroinflammatory agents for the treatment of Alzheimer's disease. Eur. J. Med. Chem. 149, 129–138.

Guo, L., Zhang, W., Li, S., Ho, C.T., 2015a. Chemical and nutraceutical properties of *Coreopsis tinctoria*. J. Funct. Foods. 13, 11–20.

Guo, Q., Cui, S.W., Ding, H., Wang, Q., Wang, C., 2015b. Non-starch polysaccharides from American ginseng: physicochemical investigation and structural characterization. Food Hydrocolloids 44, 320–327.

Habibi, Y., Heyraud, A., Mahrouz, M., Vignon, M.R., 2004. Structural features of pectic polysaccharides from the skin of *Opuntia ficus-indica* prickly pear fruits. Carbohydr. Res. 339, 1119–1127.

Heneka, M.T., Fink, A., Doblhammer, G., 2015. Effect of pioglitazone medication on the incidence of dementia. Ann. Neurol. 78, 284–294.

Hensley, K., 2010. Neuroinflammation in alzheimer's disease: mechanisms, pathologic consequences, and potential for therapeutic manipulation. J. Alzheimers Dis. 21, 1–14.

Huang, Y., Li, N., Wan, J.B., Zhang, D., Yan, C., 2015. Structural characterization and antioxidant activity of a novel heteropolysaccharide from the submerged fermentation mycelia of *Ganoderma capense*. Carbohydr. Polym. 134, 752–760.

Huang, S., Mao, J., Ding, K., Zhou, Y., Zeng, X., Yang, W., Wang, P., Zhao, C., Yao, J., Xia, P., Pei, G., 2017. Polysaccharides from *ganoderma lucidum* promote cognitive function and neural progenitor proliferation in mouse model of Alzheimer's disease. Stem Cell Rep 8, 84–94.

International Union of Pure and Applied Chemistry, 1979. Nomenclature of Organic Chemistry. Pergamon, Oxford.

Jia, X., Hu, J., He, M., Zhang, Q., Li, P., Wan, J., He, C., 2017. α- Glucosidase inhibitory activity and structural characterization of polysaccharide fraction from *Rhynchosia minima* root. J. Funct. Foods 28, 76–82.

Jiang, J., Kong, F., Li, N., Zhang, D., Yan, C., Lv, H., 2016. Purification, structural characterization and in vitro antioxidant activity of a novel polysaccharide from Boshuzhi. Carbohydr. Polym. 147, 365–371.

Jing, S., Chai, W., Guo, G., Zhang, X., Dai, J., Yan, L.J., 2016. Comparison of antioxidant and antiproliferative activity between Kunlun Chrysanthemum flowers polysaccharides (KCCP) and fraction PII separated by column chromatography. J. Chromatogr. B 1019, 169–177.

Joakim, H., Sebastian, P., Lennart, M., Oskar, H., 2013. Tau pathology and parietal white matter lesions have independent but synergistic effects on early development of Alzheimer's disease. Dement. Geriatr. Cogn. 3, 113–122.

Joshi, S.R., Eberhard, S., Nanwei, T., Parag, S., Sanjay, K., Rahul, R., 2015. Therapeutic potential of α-glucosidase inhibitors in type 2 diabetes mellitus: an evidence-based review. Expet Opin. Pharmacother. 16, 1959–1981.

Kwon, Y.I., Vattem, D.A., Shetty, K., 2006. Evaluation of clonal herbs of lamiaceae species for management of diabetes and hypertension. Asia Pac. J. Clin. Nutr. 15, 107–118.

Li, N., Yan, C., Hua, D., Zhang, D., 2013. Isolation, purification, and structural characterization of a novel polysaccharide from *Ganoderma capense*. Int. J. Biol. Macromol. 57, 285–290.

Li, N., Meng, D., Pan, Y., Cui, Q., Li, G., Ni, H., Sun, Y., Qing, D., Jia, X., Pan, Y., Hou, Y., 2015. Anti-neuroinflammatory and NQO1 inducing activity of natural phytochemicals from *Coreopsis tinctoria*. J. Funct. Foods. 17, 837–846.

Li, Q.M., Wang, J.F., Zha, X.Q., Pan, L.H., Zhang, H.L., Luo, J.P., 2017. Structural characterization and immunomodulatory activity of a new polysaccharide from jellyfish. Carbohydr. Polym. 159, 188–194.

Liu, F., Dong, B., Yang, X., Yang, Y., Zhang, J., Jin, D.Q., Ohizumi, Y., Lee, D., Xu, J., Guo, Y., 2018. No inhibitors function as potential anti-neuroinflammatory agents for AD from the flowers of *Inula japonica*. Bioorg. Chem. 77, 168–175.

Lordan, S., Smyth, T.J., Soler-Vila, A., Stanton, C., Ross, R.P., 2013. The α-amylase and α-glucosidase inhibitory effects of Irish seaweed extracts. Food Chem. 141, 2170–2176.

Nhiem, N., Tuong, N., Ky, P., Subedi, L., Park, S., Ngoc, T., Yen, P., Tai, B., Quang, T., Kiem, P., Kim, S., Kim, S., 2017. Chemical components from *Phaeanthus vietnamensis* and their inhibitory NO production in BV2 cells. Chem. Biodivers. 14, e1700013.

Pasquier, F., Boulogne, A., Leys, D., Fontaine, P., 2006. Diabetes mellitus and dementia. Diabetes Metab. 32, 403–414.

Pattanayak, M., Samanta, S., Maity, P., Sen, I.K., Nandi, A.K., Manna, D.K., Mitra, P., Acharya, K., Islam, S.S., 2015. Heteroglycan of an edible mushroom *Termitomyces clypeatus*: structure elucidation and antioxidant properties. Carbohydr. Res. 413, 30–36.

Qian, J.Y., Chen, W., Zhang, W.M., Zhang, H., 2009. Adulteration identification of some fungal polysaccharides with SEM, XRD, IR and optical rotation: a primary approach. Carbohydr. Polym. 78, 620–625.

Sahragard, N., Jahanbin, K., 2017. Structural elucidation of the main water-soluble polysaccharide from *Rubus anatolicus roots*. Carbohydr. Polym. 175, 610–617.

Sridhar, G.R., Lakshmi, G., Nagamani, G., 2015. Emerging links between type 2 diabetes and Alzheimer's disease. World J. Diabetes 6, 744–751.

Striegel, L., Kang, B., Pilkenton, S.J., Rychlik, M., Apostolidis, E., 2015. Effect of black tea and black tea pomace polyphenols on α-glucosidase and α-amylase inhibition, relevant to type 2 diabetes prevention. Front. Nutr. 2, 1–6.

Takeda, S., Sato, N., Uchioyamada, K., Sawada, K., Kunieda, T., Takeuchi, D., Kurinami, H., Shinohara, M., Rakugi, H., Morishita, R., 2010. Diabetes-accelerated memory dysfunction via cerebrovascular inflammation and Aβ deposition in an Alzheimer mouse model with diabetes. P. Natl. Acad. Sci. USA. 107, 7036–7041.

Velazquez, R., Tran, A., Ishimwe, E., Denner, L., Dave, N., Oddo, S., Dineley, K.T., 2017. Central insulin dysregulation and energy dyshomeostasis in two mouse models of Alzheimer's disease. Neurobiol. Aging 58, 1–13.

Wang, Y., Wei, X., Jin, Z., 2009. Structure analysis of an acidic polysaccharide isolated from green tea. Nat. Prod. Res. 23, 678–687.

Wang, W., Chen, W., Yang, Y., Liu, T., Yang, H., Xin, Z., 2014. New phenolic compounds from *Coreopsis tinctoria* nutt. and their antioxidant and angiotensin I-converting enzyme inhibitory activities. J. Agric. Food Chem. 63, 200–208.

Wang, T., Xi, M., Guo, Q., Wang, L., Shen, Z.M., 2015. Chemical components and antioxidant activity of volatile oil of a compositae tea (*Coreopsis tinctoria,* nutt.) from Mt. Kunlun. Ind. Crop. Prod. 67, 318–323.

Wang, C., Zhang, D., Zhang, M., Jiao, Y., Jiang, K., Yan, C., 2017a. Structural characterization of a novel oligosaccharide from *Achyranthes bidentata* and its anti-osteoporosis activities. Ind. Crop. Prod. 108, 458–469.

Wang, X., Zhang, M., Zhang, D., Wang, S., Yan, C., 2017b. An O-acetyl-glucomannan from the rhizomes of *Curculigo orchioides*: structural characterization and anti-osteoporosis activity *in vitro*. Carbohydr. Polym. 174, 48–56.

Weinstein, G., Maillard, P., Himali, J.J., Beiser, A.S., Au, R., Wolf, P.A., Seshadri, S., DeCarli, C., 2015. Glucose indices are associated with cognitive and structural brain measures in young adults. Neurology 84, 2329–2337.

Westphal, Y., Kühnel, S., Waard, P., Hinz, S.W.A., Schols, H.A., Voragen, A.G.J., Gruppen, H., 2010. Branched arabino-oligosaccharides isolated from sugar beet arabinan. Carbohydr. Res. 345, 1180–1189.

Wu, X., Jiang, W., Lu, J., Yu, Y., Wu, B., 2014. Analysis of the monosaccharide composition of water-soluble polysaccharides from *Sargassum fusiforme* by high performance liquid chromatography/electrospray ionisation mass spectrometry. Food Chem. 145, 976–983.

Yan, C., Huang, D., Shen, X., Qin, N., Jiang, K., Zhang, D., Zhang, Q., 2019. Identification and characterization of a polysaccharide from the roots of *Morinda officinalis*, as an inducer of bone formation by up-regulation of target gene expression. Int. J. Biol. Macromol. 133, 446–456.

Yao, L., Li, L., Li, X., Li, H., Zhang, Y., Zhang, R., Wang, J., Mao, X., 2015. The anti-inflammatory and antifibrotic effects of *Coreopsis tinctoria* nutt on high-glucose-fat diet and streptozotocin-induced diabetic renal damage in rats. BMC Compl. Alternative Med. 15, 314–326.

Zhang, F., Jiang, L., 2015. Neuroinflammation in Alzheimer's disease. Neuropsychiatric Dis. Treat. 14, 243–256.

Zhang, Y., Yang, X., Jin, G., Yang, X., Zhang, Y., 2016. Polysaccharides from *Pleurotus ostreatus* alleviate cognitive impairment in a rat model of Alzheimer's disease. Int. J. Biol. Macromol. 92, 935–941.

Zhao, C., Diao, Y., Wang, C., Qu, W., Zhao, X., Ma, H., Shan, J., Sun, G., 2017. Structural characters and protecting β-cells of a polysaccharide from flowers of *Inula japonica*. Int. J. Biol. Macromol. 101, 16–23.

Zhou, Y., Wang, S., Lou, H., Fan, P., 2018. Chemical constituents of hemp (*Cannabis sativa*, L.) seed with potential anti-neuroinflammatory activity. Phytochem. Lett. 23, 57–61.